




Effect of Co and Ni Contents on the Sintering Behavior, Microstructure Evolution, and Mechanical Properties of (Ti,M)C-Based Cermets

MIN CHEN,¹ XUEFENG ZHANG ^{1,2,3} XUAN XIAO,¹
and HAIQUAN ZHAO¹

1.—College of Titanium and Vanadium, Panzhihua University, Panzhihua 617000, Sichuan, China. 2.—Sichuan V and Ti Industrial Technology Institute, Panzhihua 617000, China. 3.—e-mail: wzyzxf@163.com

Binders are important components in (Ti,M)C-based cermets and affect the sintering behavior. In this study, the effect of binder content ranging from 8 wt.% to 20 wt.% on the sintering behavior, microstructure evolution, mechanical properties, and fracture morphology of (Ti,M)C-based cermets were investigated. The results indicate that the change of binder content affected the dissolution–precipitation process in the liquid-state sintering stage. When the binder content was increased from 8 wt.% to 15 wt.%, the change of core grains and rim thickness was small. The percentage of dimples increased in fracture morphology, leading to an increase in transverse rupture strength and fracture toughness. However, with the binder content further increased, more carbides dissolved in the binder and thicker surrounding rims formed, causing the mechanical properties to decrease.

INTRODUCTION

TiC-based cermets are considered as important structural materials in wear-resistant and tool applications due to their superior performances of high-temperature hardness, good chemical stability, excellent thermal deformation resistance, and so on.^{1–3} However, poor wettability of TiC by the metal binders increases the brittleness of TiC-based cermets and wide applications are limited.^{4,5} Transitional metal carbides are often added to improve the wettability and mechanical properties.^{6–9} When the secondary carbides such as WC and Mo₂C are added, (Ti,M)C-based cermets are formed where M denotes the dissolved metal elements. Binders are important components of (Ti,M)C-based cermets and mainly contribute to their toughness. Different types of Fe, Cr, Co, Ni and their compounds are selected as binders according to the specific requirements in applications.^{10,11} Fe was extensively investigated as the binder due to low costs. However, the inferior corrosion resistance becomes a challenge in

many fields.¹² It has been reported that the use of Cr as the binder increased the brittleness of cermets due to its affinity with oxygen.¹³ Intermetallic alloys such as Ti₃Al, Ni₃Al, and CrNi, and the high entropy alloys of AlCoCrFeNi, CoCrFeNiV, and so on, have also been investigated as binders to improve the comprehensive properties.^{14–17} However, the transverse rupture strength (TRS) and toughness of cermets with binders of intermetallic and high-entropy alloys are still inadequate for the cermets to be used in high-speed cutting applications.

Among the above binders, Co exhibits better wettability for the secondary carbides and Ni exhibits better wettability for TiC. Thus, Ni and Co together as binders belong to the optimum choice for obtaining (Ti,M)C-based cermets with excellent mechanical properties.^{18–22} Dong et al studied the effect of Ni/(Ni+Co) with different ratios on the microstructure and properties of Ti(C,N)-based cermets.¹⁹ They proposed that the cermet with the Ni/(Ni+Co) ratio of 0.5 had the best mechanical properties with fine microstructures. Wu et al also studied the effect of Ni/Co on the properties of Ti(C,N)-based cermets with different components.²⁰

They found that the cermet had the best properties with proper Ni/Co ratios, and that the toughness increased with a concomitant decrease in the hardness as the Ni content increased. However, the literature contains no reports on the influence of the binder content on the microstructure evolution and mechanical properties of N-free (Ti,M)C-based cermets.

In this study, TiC is used as the matrix and VC, Mo₂C, and WC are used as secondary carbides, among which VC and TiC exhibit the same crystal structure. The influence of the binder content on the shrinkage behavior, microstructure evolution, and mechanical properties of (Ti,M)C-based cermets was systematically studied.

EXPERIMENTAL

Raw Materials and Experimental Procedure

Raw materials used in this study were TiC, WC, Mo₂C, VC, Co, and Ni powders, which are commercially available with average particle sizes of 2–3 μm and a purity is > 99 wt.%. The mixtures were weighed in the mass percentage of TiC-3 wt.%, WC-3 wt.%, Mo₂C-4 wt.%, VC-x wt.%, (Co+Ni). The combined use of Co and Ni as binders with 8 wt.%, 10 wt.%, 12 wt.%, 15 wt.%, 18 wt.%, and 20 wt.% have been designated cermet A, cermet B, cermet C, cermet D, cermet E, and cermet F, respectively. At a rate of 200 rpm and in a planetary mill (QM-1SP4), the mixed powders were wet ground. The milling balls were made of WC-Co cemented carbides and the medium was alcohol. The milling time was 72 h with a ball-to-powder weight ratio of 10:1. After drying, green compacts with the dimensions of 25 mm × 8 mm × 8 mm were prepared under a pressure of 200 MPa. The pressing aid was SD-2X rubber dissolved in 120# solvent oil. (Ti,M)C-based cermets were then sintered at 1450°C under vacuum and the holding time was 1 h.

Characterization of (Ti,M)C-Based Cermets

The sintering behavior of the (Ti,M)C-based cermets was analyzed by observing the shrinkage curves on a dilatometer (NETZSCH DIL402). The equipment was first vacuumed and then injected with argon. Pressed compacts were heated to 1500°C with a rate of 5°C/min. Both the microstructure and fracture morphology characterization of the (Ti,M)C-based cermets were observed by using a TESCAN VEGA II LMU scanning electron microscope (SEM) in two modes: the backscattered electron (BSE) mode and the second electron mode. Grain size distribution of the cores was obtained by image analysis with the Image-Pro Plus 6.2 software. Distribution of metal elements in the core-rim structure was analyzed using an energy-dispersive spectrometer (EDS; Oxford INCA Energy 350). The phase identification was carried out with a step length of 0.02° in a DX-2700-type x-ray

diffractometer (XRD), which was equipped with a Cu radiation source. The operating voltage was 40 kV.

The ground cermets were prepared for mechanical tests. With a three-point bending method and on a WDW-50A mechanical properties testing machine, the transverse rupture strength tests were determined, which included five samples, with an average span of 17 mm and a loading rate of 0.5 mm/min. Densities were measured using a densitometer according to the Archimedes' method., the hardness was tested on a THV-50DX Vickers hardness tester with a load of 30 kgf and the holding time was 15 s., the fracture toughness (K_{IC}) was calculated on the basis of the indentation method, as proposed by Shetty et al.²³

RESULTS AND DISCUSSION

Analysis of Dilatometric Curves

Figure 1 shows the effect of binder contents on the sintering behavior of (Ti,M)C-based cermets. When the temperature is lower than 1100°C, the green compacts are in the solid-state sintering stage and the shrinkage ratio is small and can be ignored compared with the whole shrinkage curves. Thus, a change in the binder content exerts little effect on the solid-state sintering stage. When the heating temperature is increased further, an inflection point appears and the shrinkage rate continuously increases with increasing temperature. These results indicate that the compacts entered into the liquid-state sintering stage and the flow of the binder accelerated the densification of the compacts.²⁴ After a rapid decline, a second inflection point appeared and the shrinkage curves then shifted to a platform zone, indicating that the shrinkage of the interced cermets tended to stabilize. When the binder content was lower than 12%, the second inflection point in the shrinkage curves coincided at 1375°C. With the binder content continuing to increase, the second inflection point

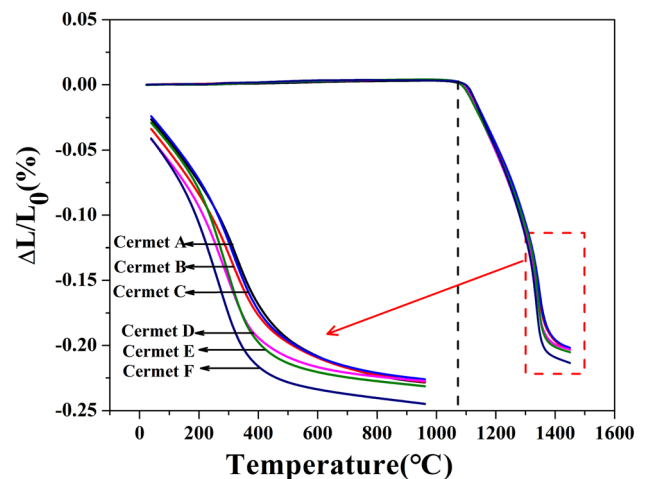


Fig. 1. Dilatometric curves of (Ti,M)C-based cermets.

gradually shifted to lower temperatures. When the amount of binder reached to 20 wt.%, the temperature at which the shrinkage curve entered the platform was the lowest. These results suggest that changing the binder content affected the liquid-state sintering stage of (Ti,M)C-based cermets and that higher binder contents are beneficial for accelerating the densification of the sintering process.

Effect of Binder Content on Microstructure Evolution of (Ti,M)C-Based Cermets

Figure 2 shows the BSE microstructures of (Ti,M)C-based cermets with different binder contents. The black cores, light-gray inner rims, and gray outer rims form a core-rim surrounding structure which is uniformly distributed in the white binders. According to the dissolution-precipitation mechanism, the solubility of TiC in a binder is lower

than that in Mo₂C, WC, and VC added carbides dissolved in the liquid-state sintering stage to reach saturation and then precipitated to form surrounding outer rims.^{25–28} The undissolved TiC grains become black cores. Inner rims formed in the solid-state sintering stage due to the diffusion of Mo₂C, WC, and VC into the TiC. The distribution difference of metallic elements between the inner rims and the outer rims cause a distinct contrast in the BSE microstructure, and thus the rims can be denoted as (Ti,M)C, where M = Mo, W, and V. Changes in the binder content influence the dissolution of the carbides and further affect the core-rim structure. Considering the distribution of metal elements in the inner rims is largely influenced by the adjacent phases, the cores and gray outer rims of (Ti,M)C-based cermets were selected for improving the accuracy of the EDS results. Table I shows

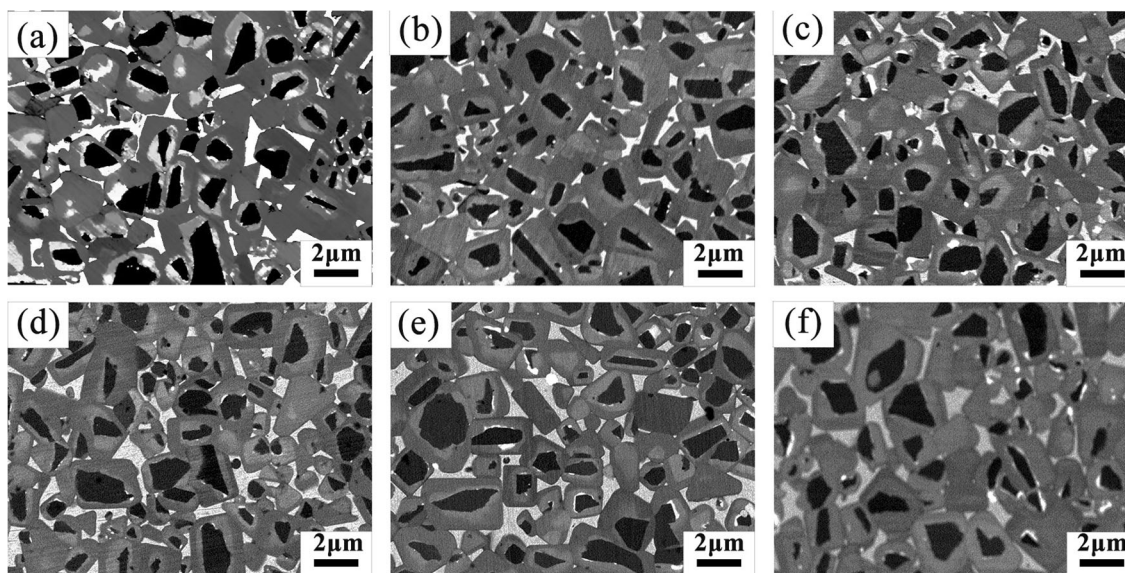


Fig. 2. BSE microstructures of (Ti,M)C-based cermets. (a) Cermet A, (b) Cermet B, (c) Cermet C, (d) Cermet D, (e) Cermet E, (f) Cermet F.

Table I. Element distribution in core-rim structure of (Ti,M)C-based cermets

Element (at.%)	Ti	V	Mo	W	Co	Ni	C
<i>Black cores</i>							
Cermet A	68.58	0.98	0.39	0.71	0.09	0.34	28.92
Cermet B	71.35	0.32	0.15	0.41	0.02	0.11	27.64
Cermet C	70.26	1.03	0.51	0.98	0.00	0.17	27.06
Cermet D	71.09	0.67	0.16	0.37	0.00	0.37	27.33
Cermet E	70.62	0.38	0.12	0.20	0.19	0.42	28.05
Cermet F	71.35	0.87	0.27	0.44	0.21	0.63	26.23
<i>Gray rims</i>							
Cermet A	64.47	2.80	1.41	2.31	0.45	2.59	25.97
Cermet B	63.46	3.27	1.55	2.76	0.18	0.25	28.53
Cermet C	63.12	3.28	1.57	2.99	0.10	0.52	28.42
Cermet D	58.69	3.36	1.63	3.16	0.75	2.69	29.72
Cermet E	58.38	3.41	1.64	3.57	1.11	3.09	28.80
Cermet F	60.62	4.07	2.11	3.76	0.89	2.25	26.30

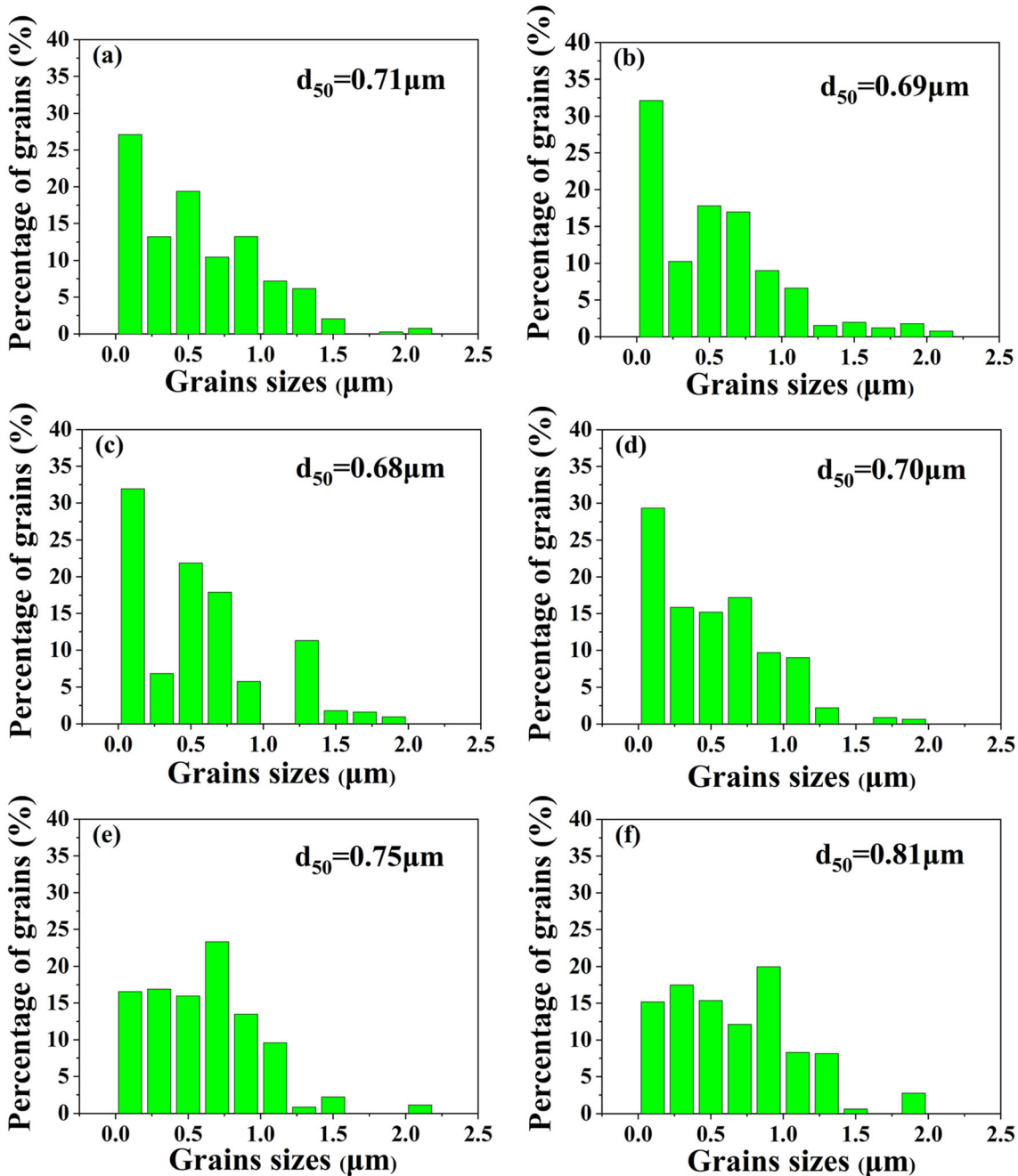


Fig. 3. Black core size distribution of (Ti,M)C-based cermets. (a) Cermet A, (b) Cermet B, (c) Cermet C, (d) Cermet D, (e) Cermet E, (f) Cermet F.

the EDS results of detected elements in the core-rim structure. The cores are mainly composed of TiC grains, and the component is less affected by a change of the binder content. V, Mo, and W are mainly distributed in the outer rims. As the binder content increases, more metal elements dissolve in the binder and then precipitate in the outer rims.

The effect of binder content on the dissolution process can be estimated based on the grain size change of the cores. Figure 3 shows the change of grain size distribution frequency and the average grain size of cores with different binder contents.

The average grain size of cores fluctuates slightly when the binder content is lower than 12 wt.%. However, higher binder contents of more than 15 wt.% result in the average grain size of the cores increasing. Based on the principle that grains of smaller carbides preferentially dissolve, the binders with higher content are beneficial for accelerating the dissolution of small TiC grains. Furthermore, the dissolution of carbides in advance reached saturation in cermets with higher binder contents, and there is more time to promote the core grains growing. As evident from the grain size distribution,

when the binder amount is more than 15 wt.%, the cores with a grain size of $< 0.25 \mu\text{m}$ account for a lower proportion, whereas the cores with a grain size of $> 0.5 \mu\text{m}$ show an increased proportion, resulting in the average grain size of the cores in cermet E and cermet F increasing.

The inner and outer rims jointly form brittle surrounding rims and their thickness plays a decisive role in the mechanical properties.²⁹ The average thickness of surrounding rims is shown in Fig. 4. Similar to the change of cores, when the binder content is lower than 12 wt.%, the average rim thickness fluctuates little. A further increase of the binder amount results in an increase in the average thickness of surrounding rims. The reasons may be explained as follows: on the one hand, according to the dilatometric curves, the binder content mainly affects the liquid-state sintering stage, additional carbides dissolve into the binder with higher content, and more (Ti,M)C precipitates in the outer rims. On the other hand, the dissolved

carbides in the binder with higher content are prone to reach saturation in advance, leading to easier growth of the precipitated (Ti,M)C grains because of the extended time in the liquid-state sintering stage.

Effect of Binder Content on the Crystal Structure of (Ti,M)C-Based Cermet

The diffraction peaks of (Ti,M)C-based cermets with different binder contents are shown in Fig. 5. Only two kinds of phases with cubic crystal structure exist in the sintered cermets, that is the carbides (Ti,M)C and the binder Co-Ni-X. X in the molecular formula Co-Ni-X is Ti, V, W, and Mo. The cores and the inner and outer rims have the same crystal structure with little difference in lattice parameters. Thus, their diffraction peaks are coincident. Notably, the (Ti,M)C diffraction peaks obviously shifted to higher angles with the binder content of higher than 15 wt.% (Fig. 1b). As is known, the atomic radius of Ti ($R_{\text{Ti}} = 0.1467 \text{ nm}$) is larger than that of V ($R_{\text{V}} = 0.1338 \text{ nm}$), Mo ($R_{\text{Mo}} = 0.1386 \text{ nm}$), and W ($R_{\text{W}} = 0.1394 \text{ nm}$). Thus, larger binder contents led to the dissolution of more carbides, which in turn increased the amount of heavy-metal carbides, causing the lattice parameters of (Ti,M)C to decrease.¹⁹ This is consistent with the increased thickness of Cermet E and Cermet F as discussed above. It is also observed that the intensity of the Co-Ni-X diffraction peaks are obviously increased with the binder content higher than 15 wt.%. Besides the increased binder content, the additional dissolved carbides are also beneficial for increasing the binder amount. The dissolved Ti, V, W, and Mo atoms in the binder are beneficial for increasing the hardness of the (Ti,M)C-based cermets via the solid solution strengthening effect.

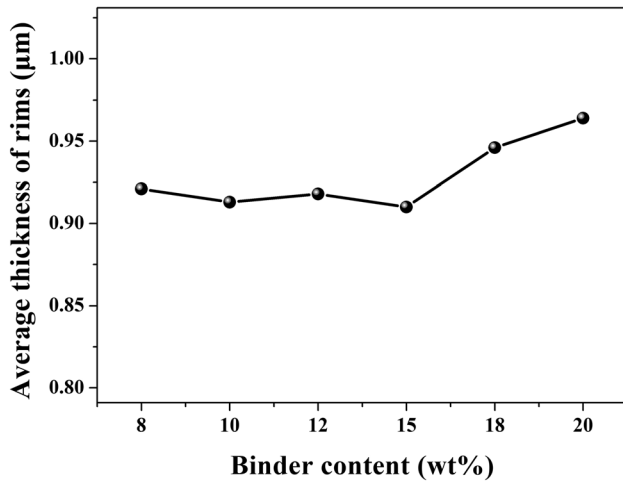


Fig. 4. Average rim thickness of (Ti,M)C-based cermets.

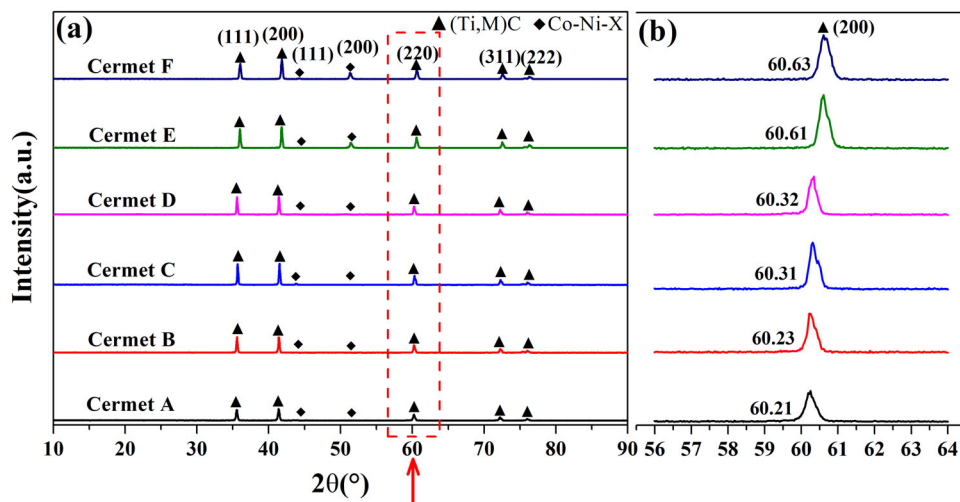


Fig. 5. (a) XRD patterns of (Ti,M)C-based cermets. (b) Enlarged view between 56° and 64° .

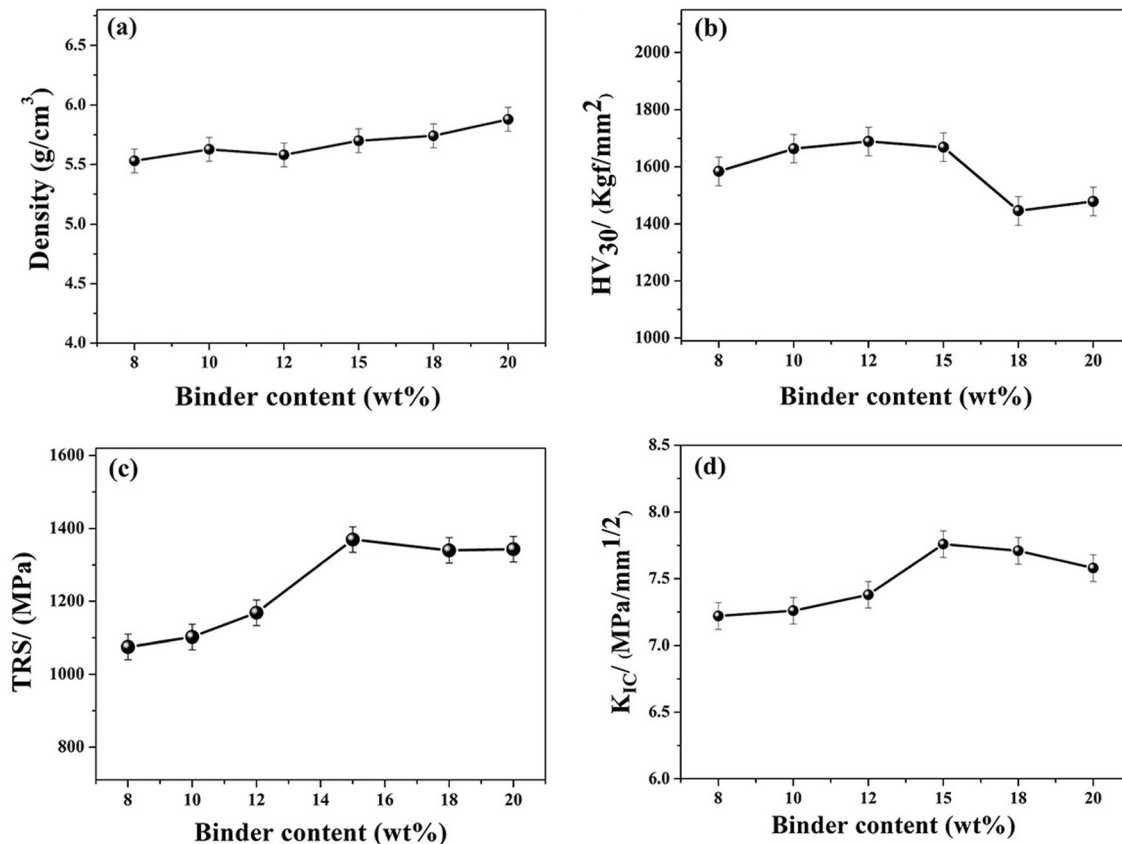


Fig. 6. Density and mechanical properties of (Ti,M)C-based cermets. (a) Density (b) Vickers hardness, (c) TRS, (d) K_{IC} .

Effect of Binder Content on Mechanical Properties of (Ti,M)C-Based Cermets

Figure 6 shows the effect of binder content on the density and mechanical properties of (Ti,M)C-based cermets. As the binder content increases, the density increases progressively due to the higher density of Co and Ni. The hardness fluctuates slightly within the binder content of 8–15 wt.% and then decreases. Theoretically, higher binder contents are beneficial for increasing the TRS and K_{IC} . However, the TRS and K_{IC} increase gradually with binder contents of lower than 15 wt.%, and do not increase any more with further increases in the binder content. As is known, the carbides mainly contribute to hardness: the more the binder content, the less carbides remain. Furthermore, the hardness of the rims is lower than that of the cores, and the increased rim thickness in Cermets E and F decreased the hardness.³⁰ With the binder content increased, the liquid-state sintering process is promoted and the wettability of the carbides by the binder is improved, which is beneficial for increasing the TRS of the (Ti,M)C-based cermets. However, when the amount of binder is more than 15 wt.%, the thickness of the surrounding rims substantially increased which is not conducive for improving the TRS. The synergistic effect of increased binder

content and rim thickness causes the TRS to no longer further increase for Cermets E and F.

To further analyze the effect of binder content on the K_{IC} of (Ti,M)C-based cermets, the fracture morphology can be seen in Fig. 7. When the binder content is low (≤ 10 wt.%), the small amount of liquid is not enough to provide good interface bonding strength, and flat cross-sections of large ceramic grains are observed, which is the typical transgranular fracture characteristics (indicated by green boxes). Compared with Cermets A and B, many dimples with intergranular fracture characteristics appeared in the fracture morphology when the binder content increased to 12–15 wt.% (red circles). The formation of dimples needs to consume more energy to pull out the ceramic particles from the binder, and thus is beneficial for increasing the K_{IC} of the (Ti,M)C-based cermets.³¹ When the binder content is 15 wt.%, the proportion of dimples is highest. As the binder content increases further, the rim thickness increases. Thick rims increases the brittleness of Cermets E and F, the transgranular fracture mode is easier to occur, and the fraction of dimples decreases, causing the K_{IC} to no longer further increase with higher binder content.

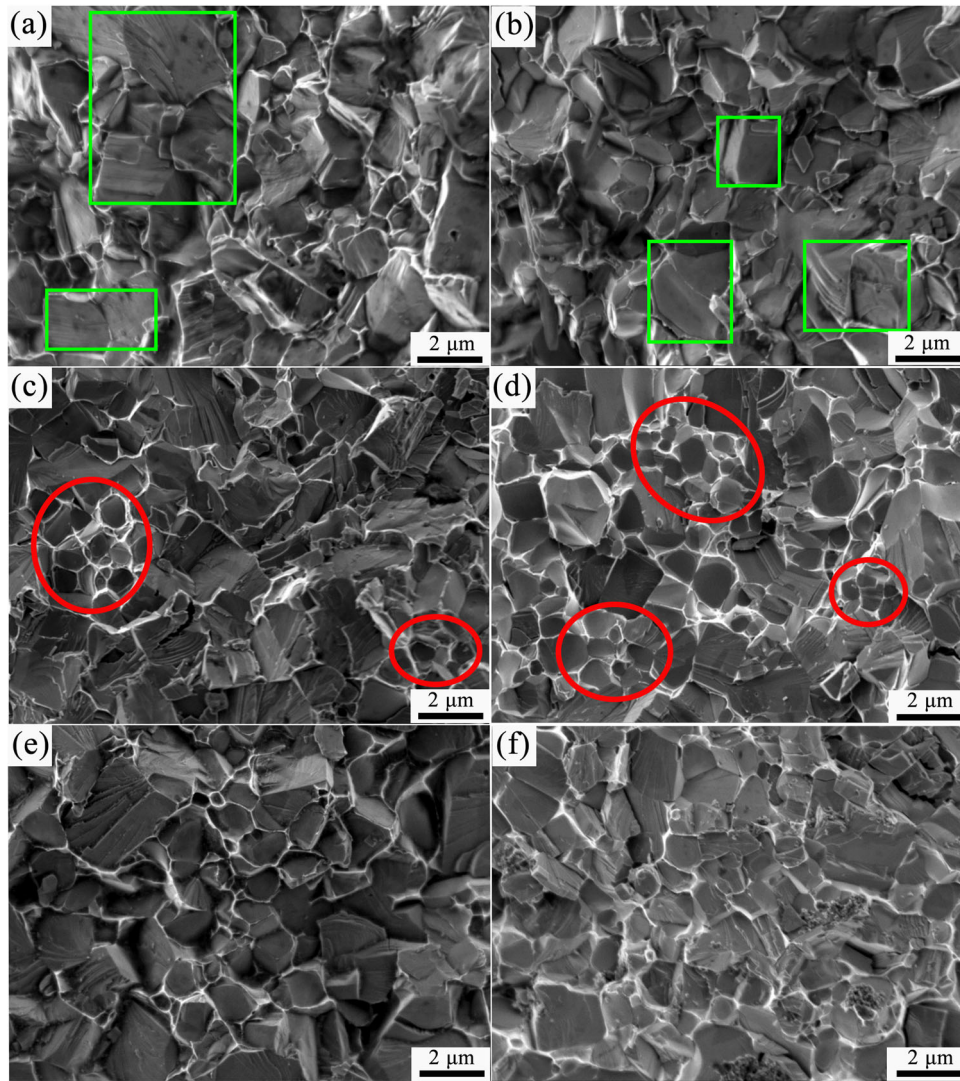


Fig. 7. Fracture morphology of (Ti,M)C-based cermets. (a) Cermet A, (b) Cermet B, (c) Cermet C, (d) Cermet D, (e) Cermet E, (f) Cermet F.

CONCLUSION

The change in binder content of (Ti,M)C-based cermets exerted limited influence on the solid-state sintering stage and the shrinkage rate could be ignored. In the liquid-state sintering stage, the shrinkage curves sharply decreased and completed the sintering process. As the binder content increased, the dissolution of carbides was promoted, and the densification of (Ti,M)C-based cermets was accelerated.

When the binder content was lower than 15 wt.%, the average grain size of the black cores decreased slowly while the surrounding rim thickness changed little. Increased binder content is advantageous to form complete core-rim surrounding structures. However, as the binder content further increased to higher than 18 wt.%, more carbides dissolved in the binder and the liquid sintering stage lasted

longer, causing the thickness of the rims to be coarsened and the average grain size of the black cores to increase. This type of microstructure adversely affected the mechanical properties.

When the binder content was low, there were cleavage planes in the fracture morphology of Cermets A and B, and the fracture mode was dominated by brittle transgranular fractures. As a result, TRS and K_{IC} values were low. When the binder content was increased to 12–15 wt.%, the fraction of dimples increased, causing the improvement of TRS and K_{IC} . (Ti,M)C-based cermets exhibited optimal mechanical properties when the binder content was 15 wt.%. However, as the binder content increased further, the TRS and K_{IC} changed little due to the synergistic effect of coarser rims and increased binder content.

ACKNOWLEDGEMENTS

The authors are grateful for the financial support by the Science and Technology Planned Project of Sichuan Province, China (No. 2020YFG0423) and the Science and Technology Planned Project of Panzhihua City, China (No. 2020CY-G-7).

CONFLICT OF INTEREST

The authors declare that they have no conflict of interest.

REFERENCES

1. A. Rajabi, M.J. Ghazali, J. Syarif, and A.R. Daud, *Chem. Eng. J.* 255, 445 (2014).
2. A.S. Rogachev, S.G. Vadchenko, N.A. Kochetov, D.Y. Kovalev, I.D. Kovalev, A.S. Shchukin, A.N. Gryadunov, F. Baras, and O. Politano, *J. Eur. Ceram. Soc.* 40, 2527 (2020).
3. A. Rajabi, M.J. Ghazali, and A.R. Daud, *Mater. Des.* 67, 95 (2015).
4. G. Li, J. Jia, Y. Lyu, J. Zhao, J. Lu, Y. Li, and F. Luo, *Ceram. Int.* 46, 5745 (2020).
5. S. Acharya, M. Debata, T.S. Acharya, P.P. Acharya, and S.K. Singh, *J. Alloys Compd.* 685, 905 (2016).
6. N. Wu, F. Xue, H. Yang, H. Zhou, Y. Li, G. Li, and F. Luo, *Mater. Today Commun.*, 25, 101311 (2020).
7. C. Liu, N. Lin, and Y.H. He, *Ceram. Int.* 42, 3569 (2016).
8. B. Liu, S. Huang, J. Van Humbeeck, and J. Vleugels, *Mater. Des.* 133, 30 (2017).
9. W. Wan, J. Xiong, and M. Liang, *Ceram. Int.* 43, 944 (2017).
10. Q. Zhuang, N. Lin, Y. He, and X. Kang, *Ceram. Int.* 43, 15992 (2017).
11. G. Li, H. Yang, Y. Lyu, H. Zhou, and F. Luo, *Int. J. Refract. Met. Hard Mater.* 84, 105031 (2019).
12. J. Kübarsepp and K. Juhani, *Int. J. Refract. Met. Hard Mater.*, 92, 105290 (2020).
13. M. Aristizabal, N. Rodriguez, F. Ibarreta, R. Martinez, and J.M. Sanchez, *Int. J. Refract. Met. Hard Mater.* 28, 516 (2010).
14. B. Huang, W. Xiong, M. Zhang, Y. Jing, B. Li, H. Luo, and S. Wang, *J. Alloys Compd.* 676, 142 (2016).
15. M. Fattahi, Y. Pazhouhanfar, S.A. Delbari, S. Shaddel, A. Sabahi Namini, and M. Shahedi Asl, *Ceram. Int.*, 46, 14105 (2020).
16. Q.C. Fan, B.S. Li, and Y. Zhang, *Mater. Sci. Eng. A*, 598, 244 (2014).
17. H. Liu, J. Liu, P. Chen, and H. Yang, *Opt. Laser Technol.* 118, 140 (2019).
18. S.M. Rafiaei, A. Bahrami, and M. Shokouhimehr, *Ceram. Int.* 44, 17655 (2018).
19. D. Dong, W. Yang, H. Xiong, L. Zhang, K. Shi, and J. Liao, *Ceram. Int.* 46, 6300 (2020).
20. L.W. Xu, N. Lin, L.B. Zhao, C. Ma, Z.Y. Wang, and Y.H. He, *Mater. Chem. Phys.*, 252, 123253 (2020).
21. Q.Z. Xu, X. Ai, J. Zhao, F. Gong, J.M. Pang, and Y.T. Wang, *J. Alloys Compd.* 644, 663 (2015).
22. H.J. Zhou, C.Z. Huang, B. Zou, H.L. Liu, H.T. Zhu, Y. Peng, and J. Wang, *Mater. Sci. Eng. A* 618, 462 (2014).
23. H. Zhou, M. Huang, H. Yang, H. Tao, Y. Yin, and F. Luo, *J. Alloys Compd.*, 843, 156072 (2020).
24. H. Xiong, Z. Li, X. Gan, L. Chai, and K. Zhou, *Mater. Sci. Eng. A* 694, 33 (2017).
25. X. Wang, Q. Wang, Z. Dong, X. Zhou, X. Wang, B. Zhang, and C. Meng, *Metals* 10, 1 (2020).
26. S. Lemboub, S. Boudebane, F.J. Gotor, S. Haouli, S. Mezrag, S. Bouhedja, G. Hesser, H. Chadli, and T. Chouchane, *Int. J. Refract. Met. Hard Mater.* 70, 84 (2018).
27. H. Xiong, Y. Wen, X. Gan, Z. Li, and L. Chai, *Mater. Sci. Eng. A* 682, 648 (2017).
28. H. Xiong, Y. Wu, Z. Li, X. Gan, K. Zhou, and L. Chai, *Ceram. Int.* 44, 805 (2018).
29. H. Zhou, C. Huang, B. Zou, H. Liu, H. Zhu, P. Yao, and J. Wang, *Int. J. Refract. Met. Hard Mater.* 47, 71 (2014).
30. Q. Xu, X. Ai, J. Zhao, H. Zhang, W. Qin, and F. Gong, *Mater. Sci. Eng. A* 628, 281 (2015).
31. W. Sun, P. Zhang, P. Li, X. She, and K. Zhao, *J. Rare Earths* 33, 867 (2015).

Publisher's Note Springer Nature remains neutral with regard to jurisdictional claims in published maps and institutional affiliations.